Annals of Nuclear Medicine Vol. 13, No. 1, 65–70, 1999

Performance stability of SHR-2000 high resolution PET for animal research

Hong ZHANG, Saleh ALYAFEI, Tomio INOUE, Katsumi TOMIYOSHI and Keigo ENDO

Department of Nuclear Medicine, Gunma University School of Medicine

The performance of a high resolution positron emission tomography (PET) system SHR-2000 for animal studies was re-evaluated six years after its installation. The system employs a detector array consisting of BGO crystals that are 1.7 mm (transaxially) by 10 mm (axially) by 30 mm (deep). A block detector, which is a position-sensitive photomultiplier tube (PMT) coupled to 4 arrays of BGO crystals has been adopted to the system. There are 15 block detectors positioned to form a 35 cm diameter ring with a field of view (FOV) of 17 cm by 4.6 cm axially, giving the system a 7 slice imaging capability. For six year workload in spatial resolution (FWHM), there were approximately a 2.6% increase at tangential FOV and a 7.5% increase at radial FOV. In axial resolution (FWHM) there was almost no change. The count rate loss for the true count rate increased 1.3% at 200 kBq/ml. The average slice sensitivity showed a decrease of approximately 4.1%, and in scatters it showed an increase of approximately 1.4%. In animal experiments, the bones of guinea pigs were clearly identified with ^{18}F fluoride ion. These experiments show that after a six year workload, the system also maintains good performance and has good stability.

Key words: animal PET, physical performance, stability

INTRODUCTION

PROGRESS in the development of new tracer kinetic models and new radiopharmaceuticals for PET, through the use of animal research, has been hindered by the limited resolution of clinical PET systems developed in the early 1980s relative to the size of the organ systems of most laboratory animals. The single slice system of Derenzo et al. has the ability to resolve many of these small structures,[1] but also has the practical limitation of being unable to examine more than a single slice in a dynamic study. A high resolution PET system (Hamamatsu SHR2000) has been installed in our laboratory for using in animal research. This block detector-based PET camera uses a position-PMT which has a high intrinsic resolution capability in both the transaxial and the axial direction.[2–4] We have used the PET system for animal research for 6 years. This paper describes the re-evaluation of the system performance of the animal PET after six years use.

Received June 3, 1998, revision accepted January 18, 1999.

For reprint contact: Hong Zhang, M.D., Department of Nuclear Medicine, Gunma University School of Medicine, 3–39–22 Showa-machi, Maebashi, Gunma 371–8511, JAPAN.

MATERIALS AND METHODS

System design

The block detector consists of a 3″ square position-sensitive photomultiplier tube (Hamamatsu R3941-02, Hamamatsu Photonics, Hamamatsu, Japan) cross-wired anodes and 4 arrays of small BGO crystals. The individual crystals have dimensions of 1.7 mm width, 10 mm height and 17 mm depth. One BGO array has 33 crystal segments with a 2 mm pitch, and 4 BGO arrays are coupled to each PMT with a 13 mm pitch. Fifteen block detectors, with a total of 1,980 crystals (495 per ring), are positioned to form a 35 cm diameter ring. The 4 rows of the BGO arrays form 4 detector rings, which provide the system with a 7 slice imaging capability. The transaxial field of view (FOV) is 17 cm in diameter and the axial FOV is 4.6 cm.

Small gaps between the individual block detectors produce diagonal blank patterns on the projection data map (sinogram), thus small angle (24°) rotation scan motion has been adopted to fill in these gaps. Non-uniformity of the detector sensitivity is averaged in the

angular direction on the sinograms by implementing the rotation scan.

The gantry has a detector ring tilt capability of ± 90°, as well as vertical ring movement of 30 cm, so that great flexibility in the subject positioning has been attained. The gantry entry diameter is 22 cm. The major aspects of the system construction are listed in Table 1.

Analog signals from each PMT are sent to a signal processing unit (SPU) by coaxial cables through a preamplifier/driver circuit mounted on each detector module. They are shortened to 400 ns by the use of the delay-line pulse clipping method. The signal from the dynode is led into the timing discriminator. The signals of the Y-direction wire anodes, which are positioned parallel to the direction of the 4 BGO arrays, are used for the energy discrimination and the determination of flashed BGO arrays.

The flashed BGO array is detected by the means of comparators. Calculation of the X-position is carried out with a charge division method using resistor chains. To improve position accuracy in the peripheral region, four signal output taps are attached to the resistor chain, and the positions are calculated in the peripheral regions separately from those in the central region.[4] The wire anode signals for the X-position are integrated and digitized through 8 bit flash analog to digital converters (ADCs), and a flashed BGO segment in the X direction is detected by a centroid calculation with a look-up-table in electrically programmable read only memory (EPROM).

Each one of 15 block detectors is in coincidence with the opposing 6 block detectors. The width of the coincidence time window can be changed electronically from 8 ns to 28 ns in steps of 4 ns and is normally set to 20 ns. The crystal pair's address including their slice address is led to an address conversion circuit card through FIFO memories, where the detector pair address is converted to a polar coordinated for sinogram formation, being combined with a detector rotation angle encoder signal.

The converted data of 180 (bins, sampled every 1.0 mm) × 225 (angles) are stored in histogram memory in a data acquisition/processing unit (DAPU). The histogram memory consists of a pair of memory bank sets, each of which has space for data acquisition (4 MB) and for the real time image monitor (256 kB).

As a main computer for the system operation and image/data processing, an engineering work station (Sun 3-80) has been adopted and software in an object oriented language smalltalk-80 environment has been developed.

Table 1 Major aspects of the system construction

Detector	
Crystal material	BGO
Crystal size	1.7 mm (w) × 10 mm (h) × 17 mm (d)
Crystal pitch	2 mm
PMT type	3″ square position sensitive PMT (Hamamatsu R3941-02)
Number of crystals	1,980 (495/ring)
Number of PMTs	15
Ring geometry	
Number of rings	4
Ring Diameter	348 mm
Ring separation	13 mm
Slice aperture	8 mm
Slice shield	47 mm (l) × 4–5 mm (w)
Opening diameter	220 mm
Gantry	
Detector ring tilt	− 90° to +90°
Detector ring elevation	300 mm
Scanning motion	Small angle rotation (24°)
Positioning	Laser projector
Source	Orbiting ^{68}Ge in capillaries

Measurements

The measurements were performed mainly based on the performance evaluation standards in positron emission tomography established by Japan Radioisotope Association and were done exactly the same in the experiments done six years ago.

Transaxial resolution was determined from the block response measurements made with a 1 mm diameter ^{18}F line source placed in air at 0, 2.5, 5, and 7.5 cm from the center of the field of view (FOV). The images were reconstructed with a Shepp-Logan filter, and the FWHM and FWTM of the profiles were determined in the radial and tangential directions by liner interpolation.

Table 2 Transaxial resolution measured with a ^{18}F line source positioned at the center, 0 and at radial position 25, 50, 75 mm apart from the center of the transaxial FOV

Source position (mm)	FWHM (mm)				FWTM (mm)			
	Tangential		Radial		Tangential		Radial	
	A	B	A	B	A	B	A	B
0	3.7 ± 0.2	3.9 ± 0.2	3.3 ± 0.2	3.5 ± 0.4	8.1 ± 0.4	8.2 ± 0.4	7.3 ± 0.6	7.3 ± 0.5
25	3.5 ± 0.2	3.7 ± 0.3	3.2 ± 0.1	3.3 ± 0.3	7.4 ± 0.4	7.7 ± 0.3	7.0 ± 0.4	7.2 ± 0.3
50	3.7 ± 0.2	3.9 ± 0.3	3.8 ± 0.0	4.0 ± 0.2	7.9 ± 0.3	8.0 ± 0.2	9.0 ± 0.3	9.1 ± 0.4
75	4.2 ± 0.2	4.2 ± 0.2	4.3 ± 0.2	5.0 ± 0.3	8.5 ± 0.6	8.9 ± 0.4	9.8 ± 0.6	10.1 ± 0.4

The values represent the means ± standard deviation across all reconstruction planes (n = 5).
A represents measured data 6 years ago and B represents the measured data now.

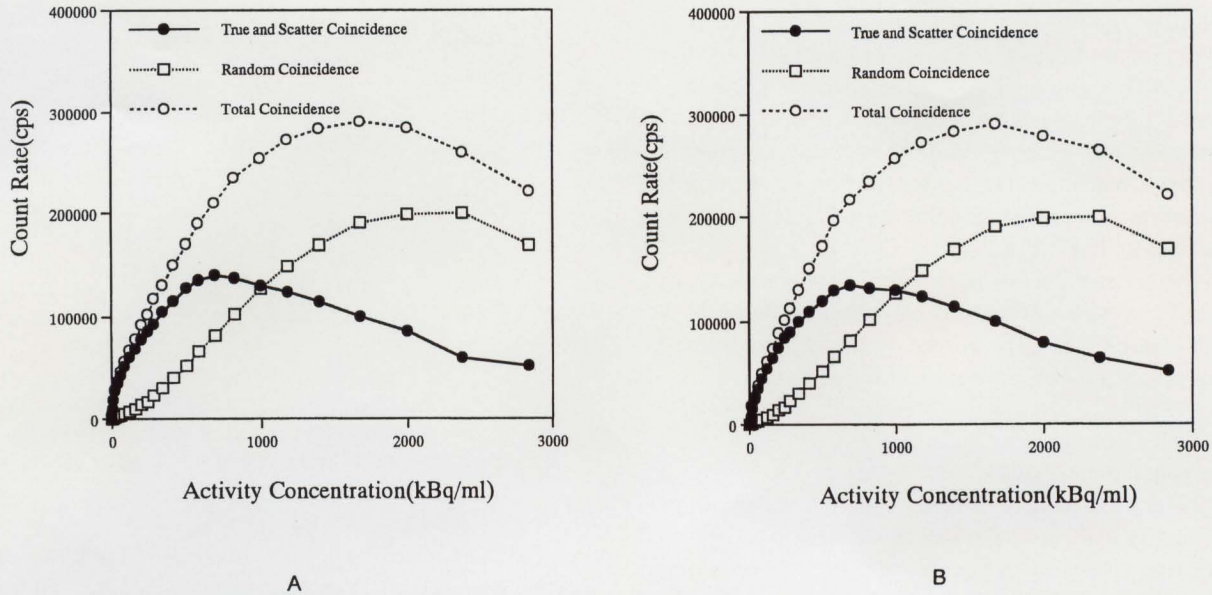

Fig. 1 Total coincidence count rate (---○---), True and Scatter coincidence count rate (—●—), Random coincidence count rate (---□---) as a function of activity concentration in a 8 cm diameter × 6.2 cm diameter height cylindrical phantom of $H_2{}^{15}O$ solution. A represents the count rate performance measured six years ago. B represents the count rate performance measured at present.

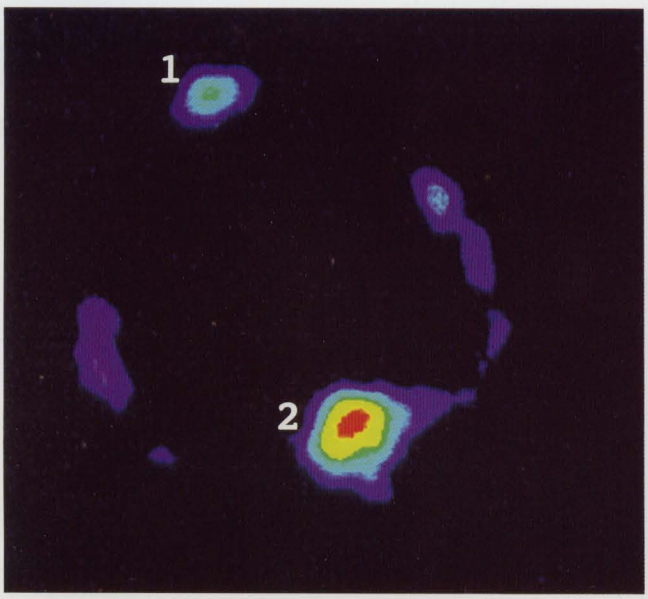

Fig. 2 Transaxial images of the thorax of the guinea pig with ^{18}F fluoride ion obtained at six years ago. Sternum (1) and vertebral body (2) were visible on PET image.

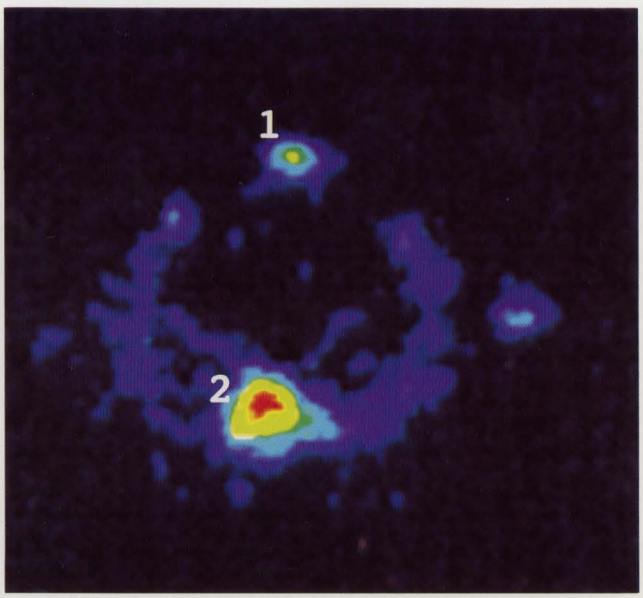

Fig. 3 Transaxial images of the thorax of the guinea pig with ^{18}F fluoride ion obtained at present. Sternum (1) and vertebral body (2) were visible on PET image.

Axial resolution was measured by scanning a 1 mm diameter ^{18}F point source in 1 mm increments, at 0 and 6 cm from the center of the transaxial FOV. The count rate of each slice was recorded at each scanning point.

Count rate performance was measured with an 8 cm diameter by 6.2 cm high cylindrical phantom uniformly filled with $H_2{}^{15}O$ solution. The initial activity was 4.91 GBq and measurements were performed for 34 minutes. The dead time correction was also performed simultaneously.

System sensitivity was measured with an 8 cm diameter cylindrical phantom filled with 13.39 kBq/m*l* of ^{18}F

solution. The true count rate per slice was recorded.

The scatter fraction was evaluated with a 16 cm diameter cylinder containing 13.98 kBq/m*l* ^{18}F solution and with a 3.2 cm diameter cylinder filled with water. The sinogram was obtained and the transaxial tomograms were reconstructed. The scatter fraction was determined as the ratio of counts in the cold area to those in the hot area in the cylinder.[5]

The experiments were performed with a 20 ns wide coincidence window and an energy window between 300 keV and 750 keV. The procedure for PET performance evaluation was the same as used six years ago.

Statistical analysis

Data are presented as the mean ± standard deviation (s.d.). Statistical analysis of difference with p value was performed by Student's t-test. All experiments were repeated five times (n = 5). A p value < 0.05 was considered significant.

RESULTS

The results of transaxial resolution measurements are summarized in Table 2, and data are presented as the mean ± s.d. across all reconstructed image planes. At the center of the transaxial FOV, the present transaxial resolution was measured and found to be 3.9 ± 0.2 mm (tangential), 3.5 ± 0.4 mm (radial) FWHM, 8.2 ± 0.4 mm (tangential) and 7.3 ± 0.5 mm (radial) FWTM, compared to 3.7 ± 0.2 mm (tangential), 3.3 ± 0.2 mm (radial) FWHM, 8.1 ± 0.4 mm (tangential) and 7.3 ± 0.6 mm (radial) FWTM, respectively six years ago. These values were degraded to 3.7 ± 0.3 mm (tangential) and 3.3 ± 0.3 mm (radial) FWHM at a radial distance of 25 mm from the center of the transaxial FOV, now with 2.6% and 7.5% increases, compared to 3.5 ± 0.2 mm (tangential) and 3.2 ± 0.1 mm (radial) FWHM before. The FWTM values were 7.7 ± 0.3 mm (tangential) and 7.2 ± 0.3 mm (radial) now, compared to 7.4 ± 0.4 mm (tangential) and 7.0 ± 0.4 mm (radial) before at the same radial position.

The tangential FWHM resolution measurements remained constant cross the remainder of the transaxial FOV, but now the radial FWHM resolution measurement had increased to 5.0 ± 0.3 mm now at a radial distance of 75 mm from the center of the transaxial FOV, compared to 4.3 ± 0.2 mm before. The tangential FWTM resolution measurements increased to 8.9 ± 0.4 mm (now) and 8.5 ± 0.6 mm (before) at a radial distance of 75 mm from the center of the transaxial FOV, and the radial FWTM value increased to 10.1 ± 0.4 mm (now) and 9.8 ± 0.6 mm (before) at the same position.

In the results of axial resolution measurements, the average axial resolution at the center of the FOV was 4.4 ± 0.4 mm FWHM and 8.5 ± 0.5 mm FWTM now, compared to 4.4 ± 0.4 mm FWHM and 8.4 ± 0.4 mm FWTM before. And, it was 5.4 ± 0.5 mm and 10.7 ± 0.5 mm FWTM at a radial distance of 60 mm from the center of the transaxial FOV now, compared to 5.4 ± 0.4 mm FWHM and 10.9 ± 1.9 mm FWHM before at the same radial position.

Table 3 Scatter fraction and sensitivity measured with phantom

Slice number	Scatter fraction		Sensitivity	
	A	B	A	B
1	13.1%	15.1%	41.2	40.0
2	15.1%	17.0%	93.2	87.7
3	15.2%	16.8%	63.5	63.3
4	14.1%	15.2%	87.5	87.0
5	16.9%	17.3%	51.2	50.2
6	17.1%	18.2%	87.5	85.0
7	18.4%	19.9%	69.5	60.3
Average	15.7%	17.1%	70.5	67.6
Total			493.6	473.5

A represents measured data 6 years ago and B represents the measured data now. (The sensitivity unit is cps/kBq/m*l*)

The results of the count rate measurements are shown in Fig. 1. The graphs show the change in the total coincidence, random and true (including scatter coincidence) rates with an increasing activity concentration. The true count rate peaks at 135,000 counts and its loss is approximately 16% at 2,000 kBq/m*l* now, compared to that of 140,000 counts and 14.7% at 2,000 kBq/m*l* before.

The results for the relative sensitivity and scatter fraction of each slice are shown in Table 3. The average relative sensitivity was 53.5 cps/kBq/m*l* for the direct plane and 86.6 cps/kBq/m*l* for the cross plane now, compared to that of 56.4 cps/kBq/m*l* and 89.4 cps/kBq/m*l* before. The average slice sensitivity was 67.6 cps/kBq/m*l*, compared to 70.5 cps/kBq/m*l* before. And the total sensitivity was 473.5 cps/kBq/m*l* including the scatter component, now, compared to that of 493.6 cps/kBq/m*l* before.

The average scatter fraction for all slices was 17.1% now, compared to that of 15.7% before.

In quantitative analysis above, comparison of spatial resolution, count rate, sensitivity and scatter fraction values showed no significant difference between the present time and six years ago (p = NS, n = 128).

Animal study

Figures 2 and 3 illustrate the imaging performance of the system with animals. Figure 2 shows a bone image of a guinea pig obtained at six years ago with ^{18}F fluoride ion. Figure 3 shows a comparative bone image obtained at the present time with the same injection dose of ^{18}F fluoride ion. Image data were collected for 30 minutes, after 30 minutes 37 MBq injection of [^{18}F]fluoride ion, and reconstructed with the Shepp-Logan filter.

DISCUSSION

To obtain the high resolution images, most of the recent commercially available PET systems use group coupling detectors, which were designed to have a large number of crystals coupled to a small number of photomultiplier tubes (PMT).[2–4] This method is cost-effective and is able to form a closely packed multi-detector ring design.[6] The smaller BGO detectors provide better spatial resolution,[1] but the spatial resolution of PET images is also limited by the size of the PMT and statistical fluctuation of the number of photons in the scintillation light reaching each PMT.[6] Kume et al. developed a block detector with a position-sensitive PMT (Hamamatsu R-3941-02) having very high intrinsic resolution.[3,7,8] The high resolution animal PET system described in this paper employs these block detectors of a position sensitive PMT coupled to 4 arrays of 1.7 mm wide BGO crystals.

The animal PET system is an important research tool for animal studies.[9] The performance and stability of the PET system directly effects the accuracy of studies and diagnosis. Quality control of the PET system is becoming a most important task.

Compared to the main physical performance of this PET system obtained six years ago, especially in spatial resolution (FWHM), there was only a small about an average 2.6% increase at tangential FOV and 7.5% increase at radial FOV. And in axial resolution (FWHM) there was almost no change for 6 years. The SHR-2000 positron camera provided quite enough high resolution PET imagings for guinea pigs and monkeys, and was almost equivalent to the 3.5 mm FWHM of the CTI713 positron camera for animal studies developed by Culter et al.[10]

The block detector used in this PET system has a limitation in count rate capability due to pulse pile-up.[7,8,11] In comparing of the count rate data, the count rate loss for true count rate events increases with approximately 1.3% at 200 kBq/m*l*, but the count rate is much lower in most animal experiments with PET. The most promising way to improve the count rate of the system is to use the positron sensitive PMTs having independent multi-anodes. In our quality control, the cross calibration was performed every week to monitor the factor changes and it showed good stability.

The average slice sensitivity was 67.6 cps/kBq/m*l*, compared to 70.5 cps/kBq/m*l* at six years ago. It showed a decrease of about 4.1%. And in scatters the average scatter fraction for all slices was 17.1% at present, compared to 15.7% six years ago—an increase of approximately 1.4%.

Figures 2 and 3 provide illustrations of the image quality attainable with the SHR-2000. Both images showed good uptake of ^{18}F fluoride ion in the sternum and vertebral body of guinea pigs, which indicate similar image characteristic quality for now and six years ago. The detail and contrast are very good for a multislice PET camera, which demonstrated the different distribution in the thorax. The sternum and thoracic spines of the guinea pig were seen on the PET images, and the fracture sites of the rib were also clearly identified on PET images of the chest.

The images of ^{18}F labeled compounds and ^{18}F fluoride ion shown in Figures 2 and 3 illustrate a type of study that will be important in the application of the SHR-2000 to basic radiopharmaceutical development. The ^{18}F fluoride ion images of the guinea pig (Figs. 2, 3) were included to provide a point of reference for the system, since the FDG metabolic scan is the most common procedure performed with PET today. The biodistribution of new radiopharmaceuticals will be an important first step in assessing the usefulness of a new compound for clinical or research applications. Biodistribution in primates also will be important in assessing the radiation dose of a compound before its application to human subjects.

In most animal PET studies, dogs and monkeys have been employed for imaging of heart and brain metabolism and neurotransmitters, but small animals such as guinea pigs, rats or even mice could be used with SHR-2000 PET due to its high spatial resolution and its stable of system performance.

CONCLUSION

The high resolution SHR-2000PET for animal studies was installed six years ago and its system performance re-evaluated. After a six year workload, the system maintained good performance, and showed good stability. This PET system is a stable and reliable tool for animal studies.

REFERENCES

1. Derenzo SE, Huesman RH, Cahoon JH. A positron tomograph with 600 BGO crystals and 2.6 mm resolution. *IEEE Trans Nucl Sci* NS-33: 659–664, 1988.
2. Uchida H, Yamashita T, Iida M, Muramatsu S. Design of a mosaic BGO detector system for positron CT. *IEEE Trans Nucl Sci* NS-33: 464–467, 1986.
3. Kume H, Muramatsu S, Iida M. Positron sensitive photomultiplier tubes for scintillation imaging. *IEEE Trans Nucl Sci* NS-33: 359–363, 1986.
4. Yamashita T, Watanabe M, Shimizu K, Uchita H. High resolution block detectors for PET. *IEEE Trans Nucl Sci* NS-37: 589–593, 1990.
5. Brooks RA, Friauf WS, Sank VJ, Cascio HE. Initial evaluation of a high resolution positron emission tomography. *J Comput Assist Tomogr* 6: 57–68, 1986.
6. Watanabe M, Uchida H, Okada H, Shimizu H, Satoh N. A high resolution PET for animal studies. *IEEE Trans Nucl Sci Symp and Med Img Conf Record*, 1648–1652, 1991.
7. Germano G, Hoffman EJ, Dahlbom M. An investigation of methods of pileup rejection for 2-D array detector employed in high resolution PET. *IEEE Nucl Sci Symposim* 2: 1263–1269, 1986.
8. Muehllehner G, Karp JS. A positron camera using positron-

sensitive detector: PENN-PET. *J Nucl Med* 27: 90–98, 1986.
9. Yukihiro M, Inoue T, Iwasaki T, Tomiyoshi K, Erlandsson K, Endo K. Myocardial infarction in rats: high-resolution single-photon emission tomographic imaging with a pinhole collimator. *Eur J Nucl Med* 23: 896–900, 1996.
10. Cutler PD, Cherry SR, Hoffman EJ, Digby WM, Phelps ME. Design features and performance of a PET system for animal research. *J Nucl Med* 33: 595–604, 1992.
11. Thompson CJ, Meyer E. The effect of live time in components of a positron tomograph of image quantification. *IEEE Trans Nucl Sci* 34: 337–343, 1987.